

1 **Synthesis, oxidation resistance and mechanical**
2 **properties of a Cr₂AlC-based MAX-phase coating on**
3 **TiAl**

4 L. Mengis^a, C. Oskay^a, N. Laska^b, M. C. Galetz^a

5 ^aDECHEMA-Forschungsinstitut, Theodor-Heuss-Allee 25, 60486 Frankfurt am Main

6 ^bDeutsches Zentrum für Luft- und Raumfahrt, Linder Höhe, 51147 Köln

7
8 <https://doi.org/10.1016/j.intermet.2023.108039>

9 **Abstract**

10 In this study, the oxidation resistance of a Cr₂AlC-based MAX-Phase coating on the Ti-48Al-2Cr-
11 2Nb (at. %) alloy was investigated at 700°C and 800°C in air. Coatings were synthesized by a
12 combination of DC magnetron sputtering and ex-situ annealing in Ar. The oxidation resistance of
13 the TiAl alloy was greatly improved due to the formation of a protective Al₂O₃/Cr₂O₃-scale at both
14 temperatures. During oxidation Al diffuses from the coating into the substrate triggered by the
15 higher Al activity of the Cr₂AlC-phase compared to the TiAl substrate. Due to the severe Al-
16 depletion Cr₇C₃, Cr₂₃C₆ as well as Cr₂Al become the predominant phases in the coating. As a result
17 of this, the very promising mechanical properties of the coated samples were negatively
18 influenced by the brittle nature of such phases leading to a decrease in the fracture strain.

19
20 **Keywords**

21 TiAl, Cr₂AlC, MAX-Phase coating, High-temperature, Oxidation, Fracture strain

23 1. Introduction

24 Intermetallic titanium aluminides (TiAl) stand out due to their combination of well-balanced
25 oxidation resistance and mechanical properties up to 700-750°C with emphasis on their excellent
26 specific high temperature strength [1]. Since more than 10 years they have been used as a high
27 temperature material for turbine blades in the low-pressure section of airplane engines [2]. The
28 formation of a mixed TiO₂/Al₂O₃-scale at high temperatures leads to a distinctive Al-depletion of
29 the metal subsurface and therefore the formation of the Z- and/or α₂-Ti₃Al phase below the oxide
30 scale dissolving higher amounts of oxygen compared to γ-TiAl [3, 4]. As it was previously shown
31 for the Ti-48Al-2Cr-2Nb alloy after thermocyclic oxidation at already 700°C [5], the material
32 successively embrittles increasing the risk of a premature mechanical failure of the affected
33 component. Researchers all around the world have been delving for appropriate high temperature
34 coatings for decades [6], however, none of them has found its way into service. This is mostly
35 caused by the negative influence of the coatings on the mechanical properties, as it is for example
36 the case for Al-rich, intermetallic coatings based on the TiAl₂- or TiAl₃-phase as exemplarily shown
37 in [7].

38 Combining characteristics of metallic and ceramic materials, ternary carbides or nitrides called
39 MAX-phases have experienced a massive increase in popularity especially within the last couple
40 of years [8, 9]. General information about this class of materials can be taken from a previously
41 published review [10]. Besides their attractive chemical, physical, and mechanical properties, they
42 show high oxidation resistance due to the formation of a protective Al₂O₃ scale for the Al-
43 containing MAX-phases [11, 12]. Ti₂AlC, Ti₂AlN as well as Cr₂AlC are the most promising
44 candidates. Accordingly, Go et al. reported the formation of dense and protective alumina scales
45 on bulk Cr₂AlC during isothermal oxidation tests at temperatures between 1000°C and 1200°C
46 [13]. Similarly, Shamsipoor et al. studied the oxidation behavior of bulk Cr₂AlC at 1000°C and
47 1100°C and observed the formation of protective α-Al₂O₃ scales and Cr₇C₃ sub-surface layers on
48 Cr₂AlC samples [14, 15]. While most of the oxidation studies were performed on bulk materials,
49 more and more publications deal with the synthesis and characterization of MAX-Phase coatings
50 for high temperature applications on different substrates [16–18]. Respective coatings were mostly
51 deposited by PVD methods, usually via magnetron sputtering [16]. After deposition, such

52 coatings are often amorphous and need to be heat treated in order to induce the crystallization of
53 the respective MAX-phase [19, 20]. While crystallization temperatures are often rather high (700-
54 900°C) for Ti_2AlC - [21] and Ti_2AlN -coatings [22], temperatures around 500-700°C are already
55 sufficient for Cr_2AlC which makes this phase a promising coating candidate for temperature- and
56 atmosphere-sensitive materials like Ti- or TiAl-based alloys as exemplarily presented by Laska et
57 al. in a recent study [23].

58 In this study, Cr_2AlC -based MAX-Phase coatings were deposited on the Ti-48Al-2Cr-2Nb (at. %) alloy by DC magnetron sputtering and ex-situ heat treatment in Ar. Oxidation tests were
59 performed at 700°C and 800°C for up to 300 h in air. Post-exposure four-point-bending tests were
60 conducted at room-temperature to investigate the influence of the coating as well as oxidation on
61 the fracture strain of the exposed samples.
62
63

64 2. Experimentals

65 The γ -based Ti-48Al-2Cr-2Nb (at. %) alloy - in the following given as “Ti4822” – was chosen as
66 the base material in this study. The alloy has a γ/α_2 -microstructure (“near- γ ”) with a very limited
67 amount of β_0 -phase at room temperature. Ingots were cut into coupons (15x10x3 mm) as well as
68 four-point-bending samples (80x6x4 mm) and manually ground down to a 1200 grit finish.
69 Coating deposition was performed at the Deutsches Zentrum für Luft- und Raumfahrt (DLR,
70 Cologne, Germany) via direct current magnetron sputtering (DC MS) using the *IMPAX 1000 HT*
71 *system* manufactured by SVS Vacuum Coating Technologie. Four pure element targets (1 x Cr, 1 x
72 Al, 2 x C) were used with a target-specific DC voltage of 1.2-3.6 kW. Before the coating deposition
73 (at 200°C, 6×10^{-3} mbar), samples were etched in an Ar-plasma (500 V, 100 kHz) in order to remove
74 the native oxide scale on the surface of the metallic samples. Using DC MS high deposition rates
75 in range of $\sim 2 \mu\text{m/h}$ were achieved, leading to overall coating thicknesses of 10-12 μm . A
76 planetary gear inside the coating chamber caused constant rotation of the samples and therefore
77 homogeneous coating deposition on all sides.

78 Heat treatment of the amorphous as-deposited coatings was performed in a silica tube under Ar-
79 flow (4 l/h) for 1 h. In order to determine the required crystallization temperature, heat treatments

80 were done between 400°C and 800°C while heating and cooling rates were 1°C/min. With the
81 employment of a wide temperature range for the heat treatment the influence of the heat
82 treatment temperature on the resulting coating microstructure was investigated and an suitable
83 annealing temperature was selected.

84 Oxidation tests were conducted in a box furnace at 700°C and 800°C for up to 300 h. Uncoated
85 samples were also exposed as a reference. After exposure durations of 100 h, 200 h, and 300 h,
86 samples were weighed using a microbalance.

87 Four-point-bending tests were performed using a universal testing rig (50 kN) at room-
88 temperature. Conversion of the recorded load-displacement values into the respective (fracture)
89 strain and stress values were used in accordance with [24] to identify the influence of oxidation
90 on the mechanical properties.

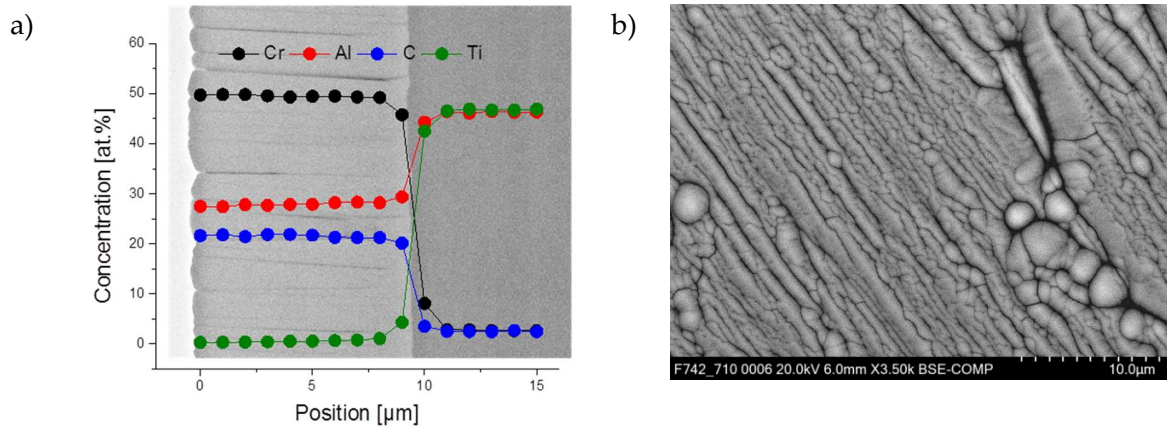
91 Before embedding (as well as gold sputtering and Ni-plating of some samples beforehand), X-ray
92 diffraction measurements (XRD, Bruker D8 Advance, Cu-K α , 10-50° (2 θ)) were performed for the
93 coated samples before and after oxidation in order to identify the phases in the annealed coating
94 prior to oxidation as well as the thermally grown oxide scale. Using SEM (Philips XL40 and
95 HITACHI SU500) and EPMA (JEOL JXA-8100) further information on the morphology of the
96 oxide scales, microstructure of the coating, and relevant interdiffusion phenomena were gathered.
97 Nanoindentation measurements (NHT2, Anton Paar) were performed using a diamond
98 Berkovich-type indenter on the cross-section with a maximum load of 20 mN to determine the
99 indentation hardness and modulus of the coating in the annealed condition.

100 **3. Results**

101 *3.1. Coating synthesis*

102 Figure 1a shows a BSE image of a cross-section of the amorphous Cr/Al/C-coating along with its
103 chemical composition measured by EPMA. The coating has a thickness of around 10 μm , good
104 adhesion to the substrate, and a homogeneous chemical composition. Mean Cr-, Al-, and C-
105 concentrations are 49.5 at. %, 27.9 at. %, and 21.6 at. % (determined from the EPMA line scan).

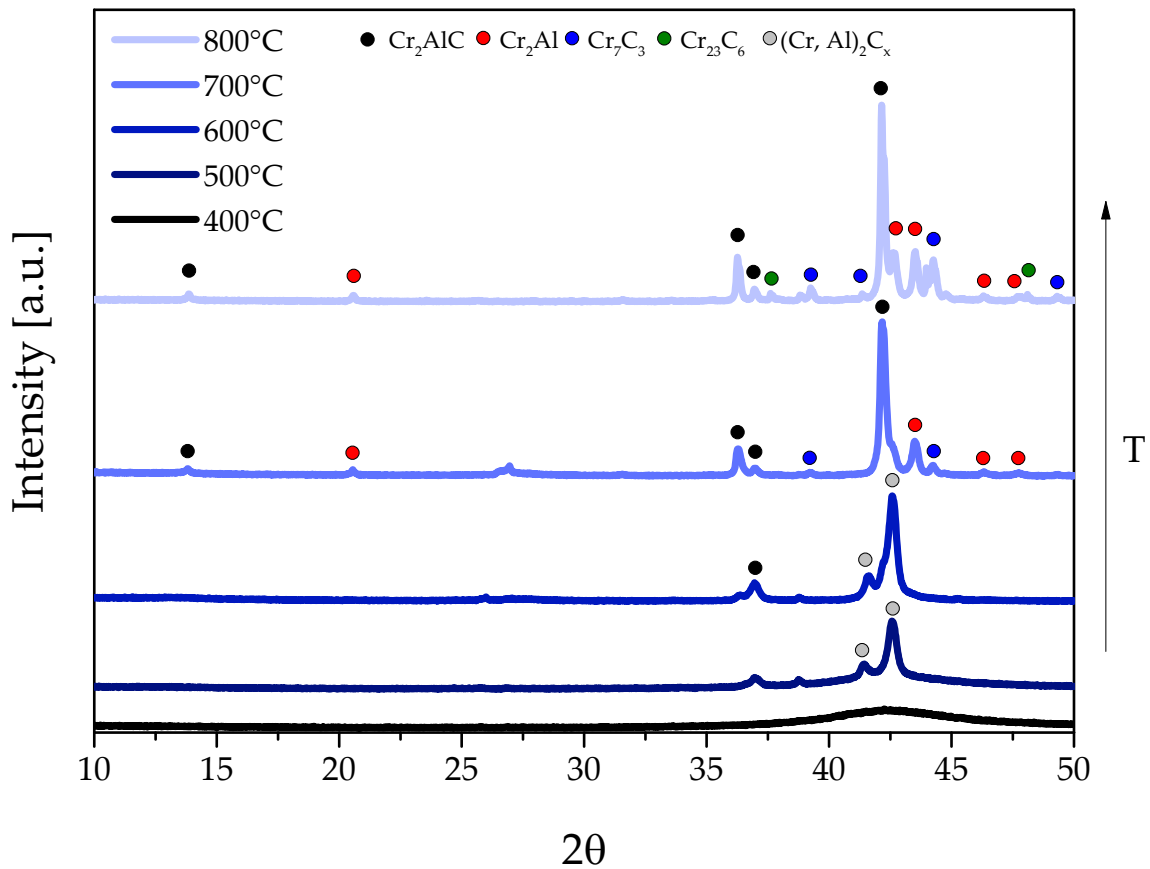
106 Figure 1b reveals the columnar microstructure of the coating typical for the MS process at rather
107 low temperatures according to the well-known Thornton model [25].



108 **Figure 1:** Back-scattered electron (BSE) images of a) a cross-section of the amorphous Cr/Al/C-coating on
109 the Ti4822 alloy with chemical composition (EPMA) and b) the surface top view of the Cr/Al/C-coating.

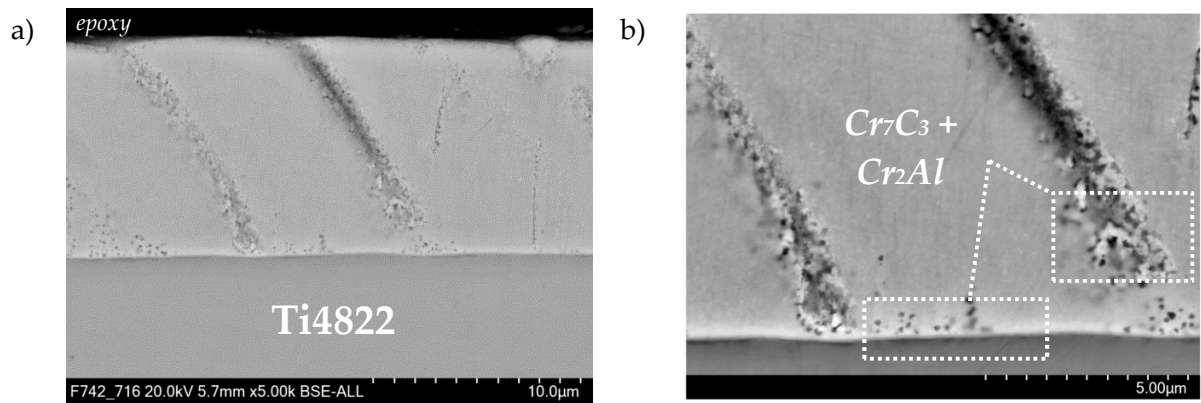
110 XRD measurements were performed before and after the heat treatment in Ar in order to identify
111 the required crystallization temperature. Results are summarized in Figure 2. While the coating is
112 still amorphous after heat treatment at 400°C, a $(\text{Cr, Al})_2\text{C}_x$ solid solution starts to form at 500°C.
113 Increasing the temperature up to 600°C leads to the formation of the first distinctive Cr_2AlC -reflex.
114 However, the $(\text{Cr, Al})_2\text{C}_x$ -phase still exists indicating an incomplete phase transformation. Further
115 Cr_2AlC -reflexes are clearly visible at 700°C, whereas the solid solution disappeared. The Cr_2AlC -
116 phase, binary Cr_7C_3 as well as the intermetallic Cr_2Al phase exist while the Cr_{23}C_6 phase
117 additionally forms with increasing temperature further to 800°C.

118



119
 120 **Figure 2:** XRD pattern of the Cr/Al/C-coating after heat treatment between 400°C and 800°C for 1 h in Ar.
 121 The Powder Diffraction File™ (PDF®) database numbers used for the reflex identification are: 29-0017, 29-
 122 0016, 11-0550, 14-0407 for the Cr₂AlC, Cr₂Al, Cr₇C₃, Cr₂₃C₆, respectively. For the identification of the reflexes
 123 of the (Cr,Al)₂C_x phase, the XRD diffractogram in [19] was used.

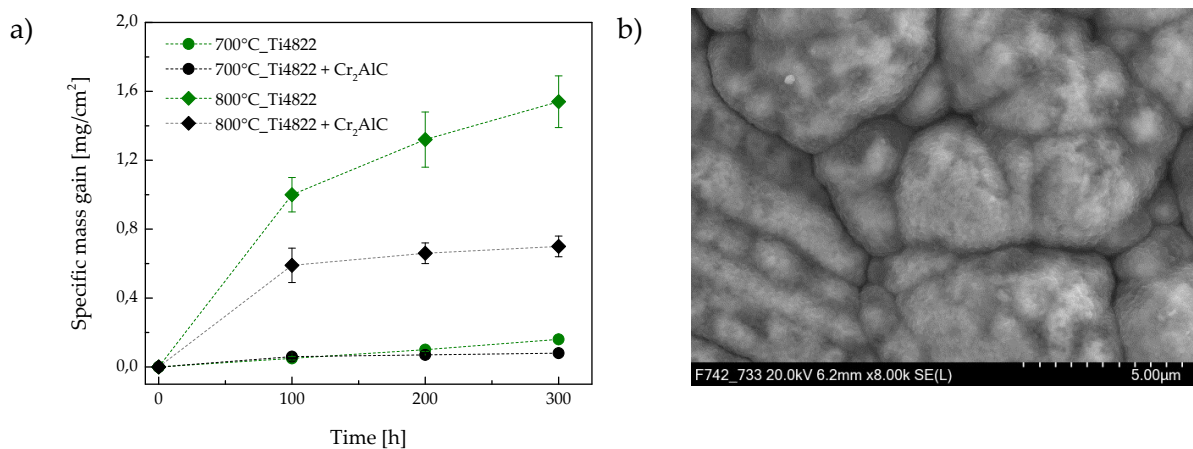
124 Based on the XRD-results, a heat treatment at 700°C for 1 h was chosen as the most promising
 125 procedure regarding the coating phases and depicts the initial condition for the oxidation tests
 126 presented in the further course of this study. Figure 3 shows the respective cross-section of the
 127 coated Ti4822 alloy after heat treatment at 700°C. The columnar microstructure can still be
 128 identified while the extent of columns has clearly decreased. At the interface between the
 129 columnar grains and the inter-columnar cavities as well as at the coating/substrate-interface
 130 precipitation of very fine Cr-carbides and the Cr₂Al phase can be observed, as illustrated in Figure
 131 3b.



132 **Figure 3:** BSE- image of the a) Cr₂AlC-based coating on the Ti4822 alloy after heat treatment at 700°C for 1
 133 h in Ar with b) magnification of the coating/substrate-interface showing precipitation of Cr₇Cr₃ and Cr₂Al.

134 **3.2. Oxidation resistance**

135 The results of the isothermal oxidation tests are presented in Figure 4. Both, the uncoated and
 136 coated Ti4822 alloy show very low specific net mass gains at 700°C. At 800°C, the positive
 137 influence of the Cr₂AlC-based coating on the oxidation behavior becomes way more pronounced.

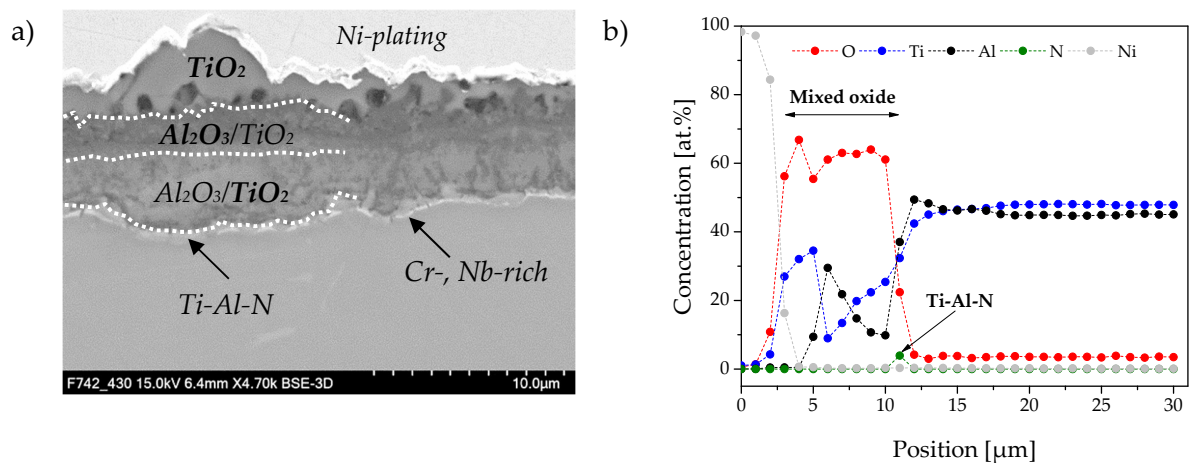


138 **Figure 4:** a) Specific net mass change of the uncoated and coated Ti4822 alloy after oxidation at 700°C and
 139 800°C in air with b) SE-image of the surface of the coated Ti4822 alloy after oxidation at 800°C for 300 h in
 140 air.

141 While the uncoated alloy already shows a mass gain of 1.54 ± 0.2 mg/cm², the respective mass gain
 142 of the coated samples is only 0.7 ± 0.1 mg/cm². Only a very thin oxide scale has formed on top of
 143 the coating and its initial columnar characteristic is still clearly visible (Figure 4b). For the

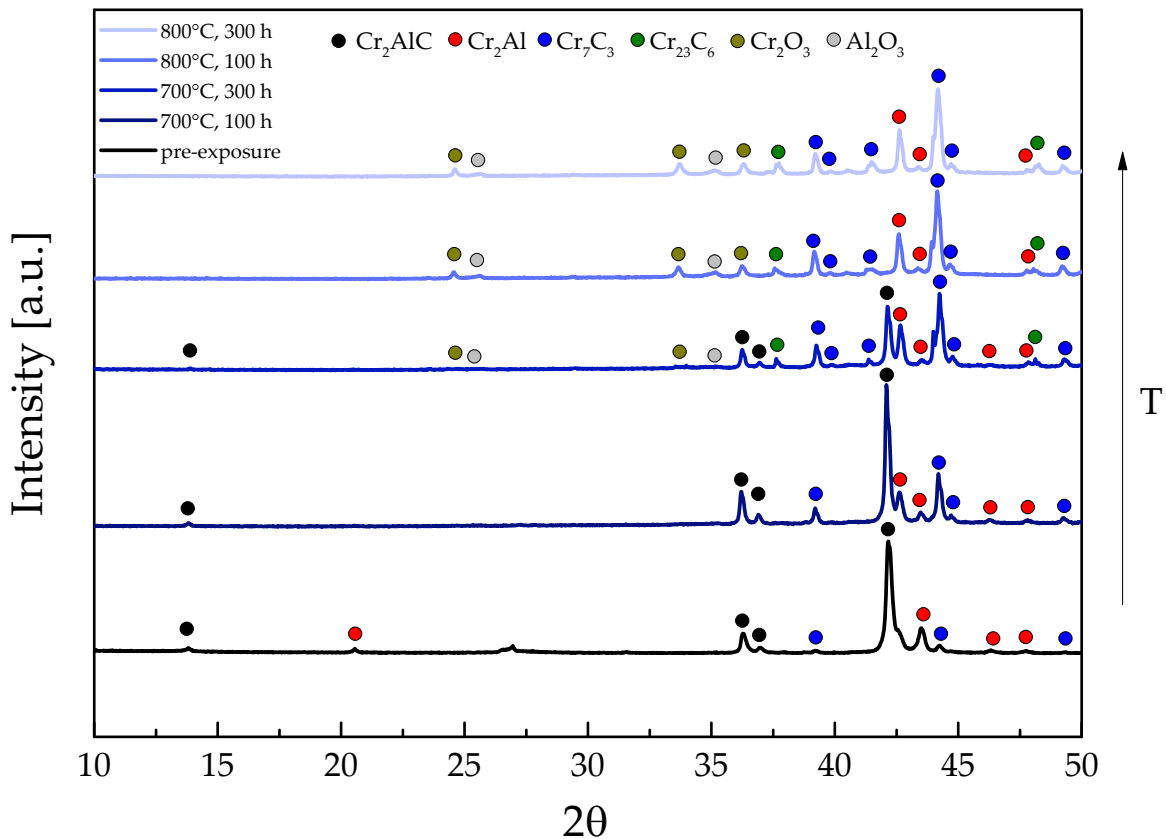
144 uncoated Ti4822 alloy a mixed $\text{TiO}_2/\text{Al}_2\text{O}_3$ oxide scale formed at both temperatures. Figure 5
 145 exemplarily shows a cross-section of the uncoated alloy after oxidation at 800°C for 100 h with the
 146 respective chemical composition measured by EPMA. The oxide scale is characterized by the
 147 typical layered structure of alternating TiO_2 and Al_2O_3 as well as a continuous Ti-A-N-layer at the
 148 interface to the substrate caused by nitrogen ingress during oxidation. In addition, Cr- and Nb-
 149 rich precipitates have formed at the interface. Since the oxidation behavior of TiAl alloys is well
 150 investigated the focus of this study is placed on the characteristics of the MAX-phase coating, an
 151 no further analysis of the cross-sections of the uncoated material is presented here.

152



153 **Figure 5:** a) BSE-image of the uncoated Ti4822 alloy after oxidation at 800°C for 100 h in air with b)
 154 corresponding EPMA line scan.

155 Figure 6 illustrates the XRD-pattern for the coated samples after oxidation at 700°C and 800°C in
 156 comparison to the initial condition (pre-exposure). While there is no large deviation in the phase
 157 composition between the pre-exposure condition and the samples oxidized at 700°C for 100 h,
 158 Cr_2O_3 and Al_2O_3 reflexes with low intensities appear after oxidation at 700°C for 300 h and reflexes
 159 of the Cr_2AlC -phase are still present. This is not the case at 800°C . Cr_2AlC -reflexes are no longer
 160 visible and the intensities of the binary Cr-carbides as well as the Cr_2Al phase increase already
 161 after oxidation for 100 h. It is important to note that, there is no sign of TiO_2 -formation for the
 162 coated alloy. Al_2O_3 and Cr_2O_3 are the only oxide phases which were detected by XRD.

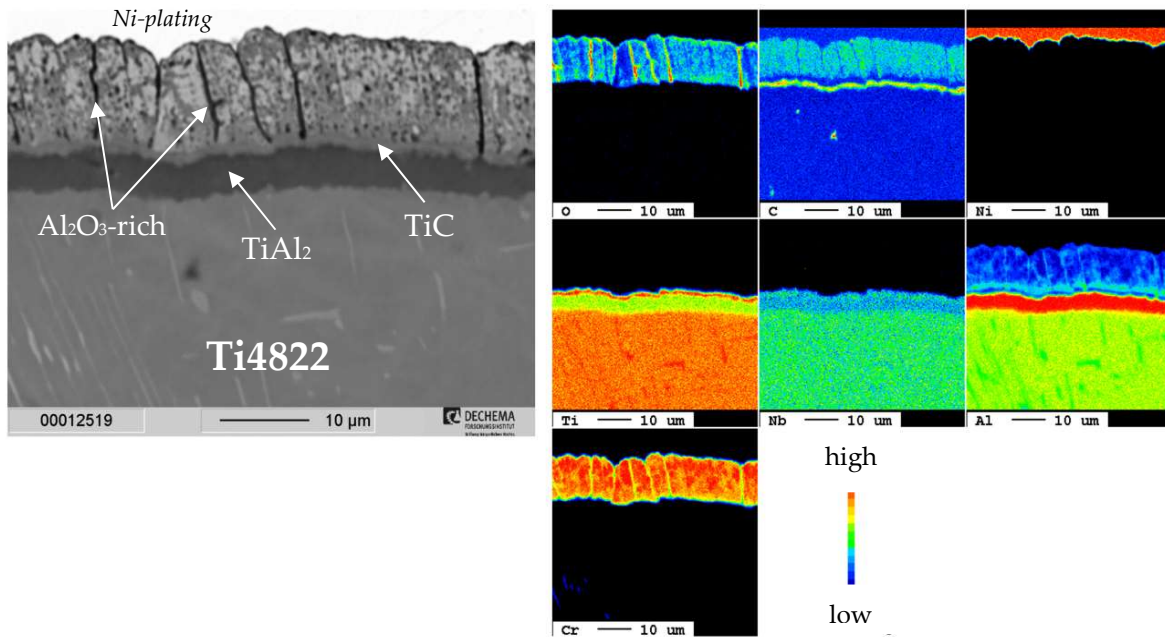


163
 164 **Figure 6:** XRD pattern of the Cr₂AlC-based coating after exposure at 700°C and 800°C in comparison to the
 165 initial condition (pre-exposure). The Powder Diffraction File™ (PDF®) database numbers used for the reflex
 166 identification are: 46-1212 and 38-1479 for Al₂O₃ and Cr₂O₃ phases (see Figure 2 for the database numbers
 167 belonging to coating phases).

168 Figure 7 depicts the coated Ti4822 alloy in combination with the EPMA-element maps after
 169 exposure for 300 h at 700°C. The inter-columnar cavities were filled with Al₂O₃. Besides the former
 170 cavities, the high oxygen signal in the coating likely originates from the high amount of
 171 nanoporosity along with being a well-known feature of the MS-technique since internal oxide
 172 formation cannot be fully precluded. An extremely thin, via EPMA line scan barely detectable
 173 oxide scale covers the coating while an Al₂O₃-rich layer has also formed along the former columns
 174 during oxidation. Severe Al-inward diffusion into the substrate led to the formation of a TiAl
 175 layer in the metal subsurface as well as Al-depletion of the coating. Due to the Al-depletion, Cr-
 176 carbides become even more prominent – especially along the columns as well as the outermost

177 part of the coating - which can already be seen in the BSE-image due to the different contrasts.
178 There is no evidence for Cr-inward diffusion. At the coating/substrate-interface, a continuous TiC-
179 layer had formed due to carbon ingress into the substrate.

180

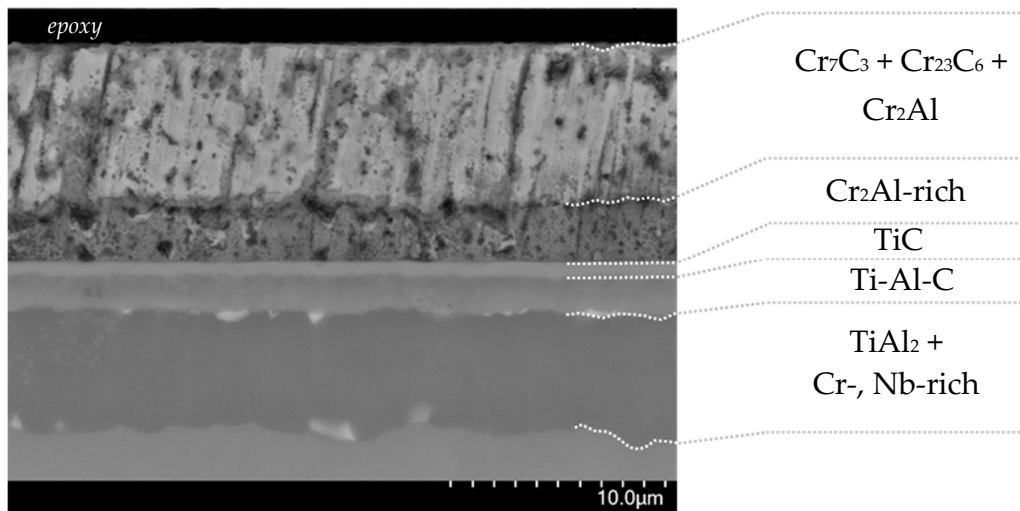


181

182 **Figure 7:** BSE-image and corresponding EPMA-element maps of the coated Ti4822 alloy after oxidation at
183 700°C for 300 h in air.

184 Above-described characteristics become even more pronounced after oxidation at 800°C for 300 h
185 as can be seen in Figure 8. The coating is still covered by an extremely thin and highly protective
186 oxide scale. Al-consumption due to oxide formation as well as Al inward diffusion in the base
187 material led to an extensive Al-depletion of the coating and the stabilization of the Cr-carbides in
188 the outermost part of the coating. A 3-4 μm thick Cr₂Al-rich layer is stable at the interface while a
189 reaction between TiC and TiAl₂ led to the formation of a ternary Ti-Al-C layer in between. Nb-
190 and Cr-rich phases have precipitated along the phase boundaries of the TiAl₂ layer.

191



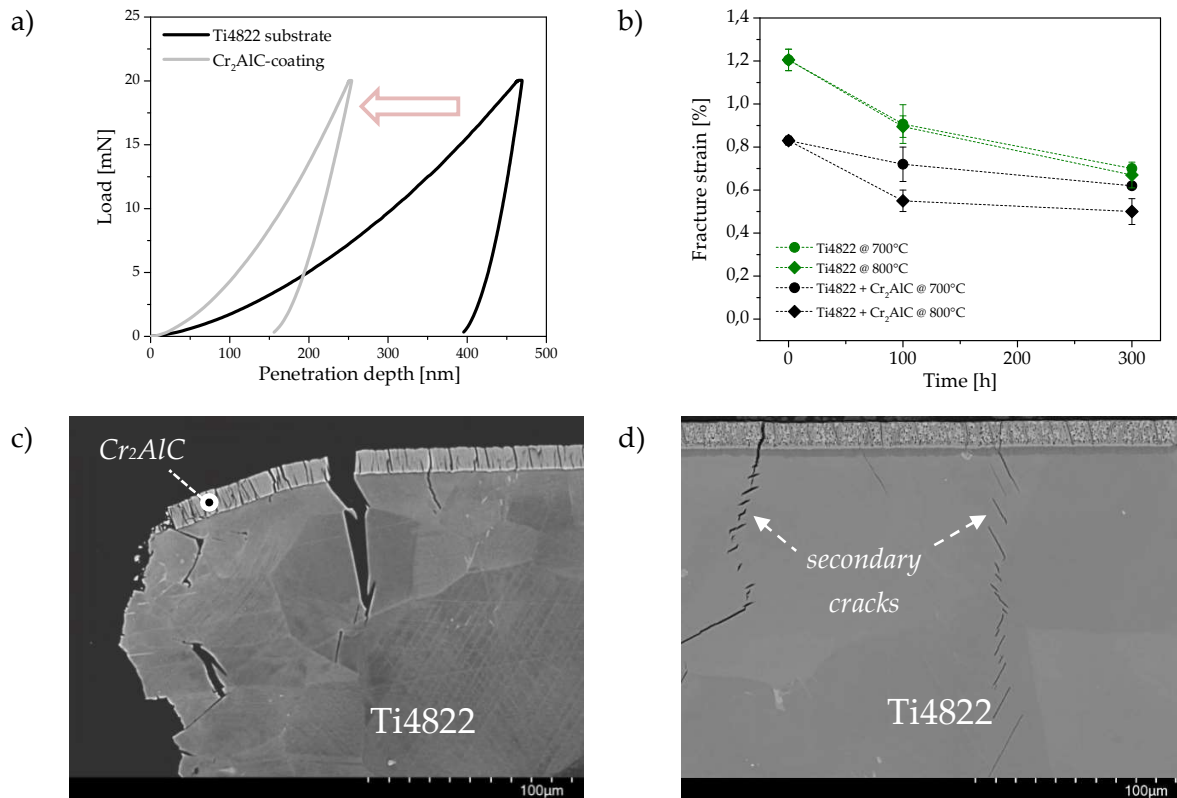
192
 193 **Figure 8:** BSE image of the coated Ti4822 alloy after oxidation at 800°C for 300 h with identified phases. The
 194 illustration of the extremely thin Cr₂O₃+Al₂O₃-scale on top of the coating was purposely omitted.

195 3.3. Mechanical properties

196 The Cr₂AlC-based coating has an indentation hardness of 15.3 ± 3.6 GPa being much higher than
 197 the one for the Ti4822 base material (4.2 ± 0.4 GPa) and leads to even lower penetration depths
 198 during the indentation measurements exemplarily shown in Figure 9a. The indentation modulus
 199 increases from 181.7 ± 12.0 GPa (Ti4822) to 254.0 ± 21.8 GPa (Cr₂AlC).

200 The results of the four-point-bending tests are summarized in Figure 9b. The uncoated Ti4822
 201 alloy has a fracture strain of 1.21 % in the as-received condition. Oxidation at 700°C and 800°C for
 202 300 h leads to a severe decrease down to 0.70% (reduction of ~43 %) and 0.67 % (reduction of ~45
 203 %), respectively. The mechanical properties are negatively affected already after oxidation for
 204 only 100 h at both temperatures. This can be explained by microstructural changes and oxygen
 205 uptake. For details the reader is referred to previously published work [26] identifying potential
 206 reasons for the embrittlement of TiAl at different temperatures.

207



208 **Figure 9:** a) Load-displacement curves of the Ti4822 substrate and the Cr₂AlC-based coating after annealing;
 209 b) Fracture strain values of the coated and uncoated Ti4822 alloy before and after oxidation at 700°C and
 210 800°C as a function of time with respective BSE-images of the coated samples after four-point bending tests
 211 at room-temperature for the c) pre-exposure condition and d) after oxidation at 700°C for 300 h in air.

212 The Cr₂AlC-coated samples show an average fracture strain of 0.83 % in the annealed condition.
 213 As for the uncoated alloy, oxidation leads to a decrease in the fracture strain at both temperatures.
 214 After oxidation at 700°C for 300 h the values become comparable to the values of uncoated
 215 samples, while oxidation at 800°C leads to the lowest fracture strain values (0.5 %) of all samples
 216 tested. Figure 9c and d illustrate the fracture behavior for the coated samples before and after
 217 oxidation. Cracks are mainly initiated between the columns and proceed along them until they
 218 reach the coating/substrate-interface. Hereby, cracks are deflected and run into to substrate in a
 219 transgranular zig-zag manner. The same characteristics can be observed for the samples exposed
 220 at 700°C for 300 h (Figure 9d). Noticeably, coatings show excellent adherence and no sign for
 221 delamination under tensile load for both, the pre-exposed and exposed condition.

222 4. Discussion

223 4.1. Coating synthesis

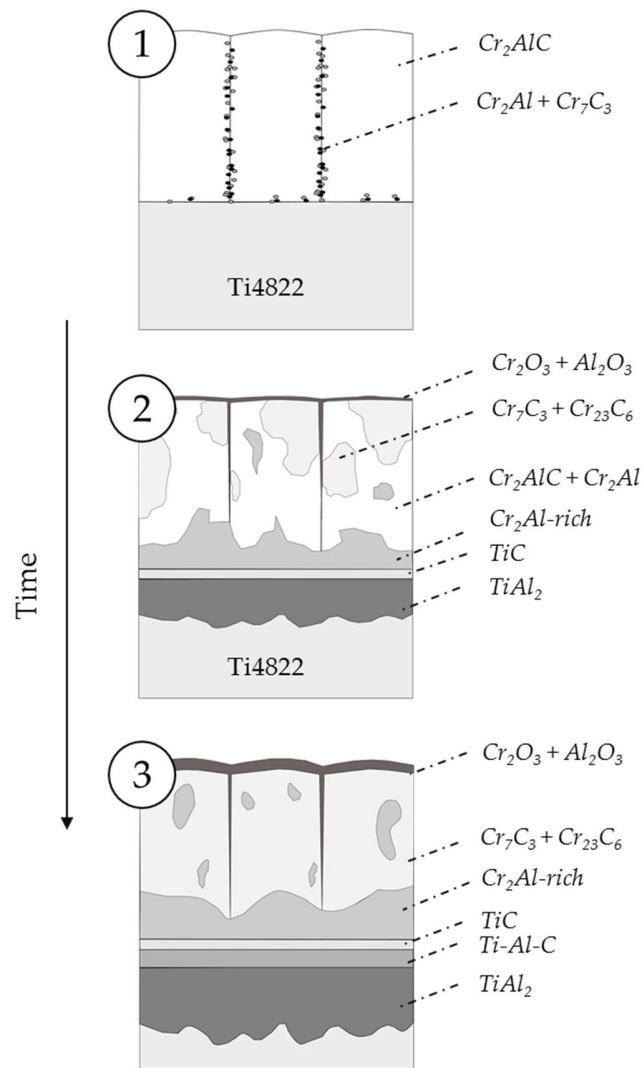
224 Based on the XRD results shown in Figure 2 coating synthesis of a Cr₂AlC-based MAX-phase
225 coating was performed by a combination of DC magnetron sputtering and an ex-situ heat
226 treatment at 700°C for 1 h in Ar. The Cr₂AlC MAX-phase was generally chosen as a promising
227 coating candidate for TiAl alloys due to their good high temperature properties as well as its
228 rather low crystallization temperature. Besides its high oxidation resistance and low
229 crystallization temperature, Cr₂AlC possesses a similar coefficient of thermal expansion (CTE,
230 reported values of 11·10⁻⁶ K⁻¹ [13] and 13·10⁻⁶ K⁻¹ [27]) as the γ-TiAl alloys (exemplarily for TNM
231 alloy around 11·10⁻⁶ K⁻¹ at approximately 600°C [28]). This good match of CTEs can lead to a low
232 intensity of thermally induced stresses in the coating and thereby reducing the coating damage
233 during thermocyclic exposure. The coating deposition temperature should be as low as possible
234 for Ti- and TiAl-based alloys to maintain the initial microstructure which can be affected by minor
235 oxygen uptake during coating deposition. While for Ti₂AlC or Ti₂AlN rather high temperatures
236 are required, Cr₂AlC-coatings were shown to crystallize already at around 500-700°C which is in
237 good agreement with the results of this study. Since coatings thickness can have an influence on
238 the crystallization kinetics [29], it has to be mentioned, that in contrast to our study, investigations
239 on the synthesis on MAX-phase coatings are very often performed on rather thin layers [30], [31].
240 In [19] and [32], the intermediate existence of the (Cr, Al)₂C_x solid solution was proven which
241 occurred after heat treatment for 500°C and also 600°C in our study. In addition to the Cr₂AlC-
242 phase, Cr₇C₃ and the intermetallic Cr₂Al-phase formed (Figure 3) especially along the columns as
243 well as the interface to the substrate. Unlike for bulk materials, the deposition of single-phase
244 coatings is a major challenge for MAX-phase coatings as described in various studies [33-35]. This
245 is due to the small stability range of the MAX-Phases which can already be deduced from the
246 ternary Ti-Al-C- or Cr-Al-C-phase diagrams [36]. In [37] it was exemplarily shown, that small
247 deviations from the stoichiometric composition (e.g. by a too low Al-content) can lead to the
248 formation of additional phases, in this case Cr₂₃C₆ and/or Cr₂Al. A certain amount of Al-depletion
249 already occurs during the ex-situ heat treatment by minor Al-oxide formation (blueish color of

250 the sample) and Al-inward diffusion into the base material (thin, dark layer in Figure 3b). This
251 phenomenon becomes even more pronounced at 800°C and induces the additional formation of
252 Cr₂₃C₆ (Figure 2). Nanoporosity and oxygen uptake during manufacturing triggers internal
253 alumina formation and additionally changes the composition and thus phases in the coating.

254 *4.2. Oxidation performance*

255 During oxidation at 700°C and 800°C, Al₂O₃ and Cr₂O₃ form on the coated material (Figure 6)
256 whereas an unprotective, thick TiO₂+Al₂O₃-scale covered the uncoated Ti4822 alloy (Figure 5). The
257 formation of an intermixed oxide scales with high oxidation kinetics above 700°C on TiAl is
258 already reported in various studies [38–40] and caused by the nearly identical thermodynamic
259 stabilities of Ti/TiO and Al/Al₂O₃ [41] in combination with the high growth rates of rutile [42].
260 Despite the high Al-content (43-48 at. %) of the commercial alloys, TiAl alloys do not exclusively
261 form Al₂O₃ scales due to their low aluminum activity. Regarding this aspect, the reader is referred
262 to [26], [43], [44] in which the oxidation behavior of the Ti4822 alloy is already described in detail.
263 The oxidation behavior of a Cr₂AlC has already been investigated e.g. in [45]. In [11] it was
264 reported that Cr₂AlC forms a protective Al₂O₃-scale between 700°C and 1000°C which is
265 associated with the formation of a Cr₇C₃-layer below the oxide due to the successive Al-
266 consumption. For the Cr₂AlC-coating only a couple of studies exist, however, the formation of
267 Cr₂O₃ was rarely mentioned [46]. The co-existence of Cr₂O₃ and Al₂O₃ in this study can presumably
268 be explained by the existence of Cr-carbides which are present after the heat treatment and
269 inevitably oxidize to Cr₂O₃ under the release of carbon which can either react with the substrate
270 to form the observed TiC and TiAlC or be oxidized to CO₂. Due to the formation of a first, very
271 thin oxide scale in the initial period of oxidation, the oxygen partial pressure decreases at the
272 oxide/coating-interface and Al₂O₃ becomes the most stable oxide in accordance with the
273 Ellingham-Richardson-diagram. The formation of Cr₂O₃ can also be positive in terms of the overall
274 oxidation resistance since it can accelerate the transition from metastable γ- or θ-Al₂O₃ to the slow-
275 growing, well protective α-Al₂O₃ because both oxides share the same crystal structure ((Cr,
276 Al)₂O₃) [47]. All in all, very thin oxides scales have formed since they are barely visible in the
277 respective SEM-images in Figure 7 and Figure 8 leading to the overall very promising oxidation
278 resistance (Figure 4).

279 Figure 10 illustrates the proposed oxidation mechanism of the Cr₂Al-based coating on TiAl as
280 function of time at a constant temperature. The high-temperature exposure of the coated Ti4822
281 alloy goes along with severe Al-inward diffusion into the substrate (Figure 7). This leads to the
282 stabilization of the Cr₇Cr₃, Cr₂₃C₆, and Cr₂Al-phases in the outer part of the coating as well as the
283 formation of a rather thick TiAl₂-layer in the metal subsurface as it is shown in Figure 8 after
284 oxidation at 800°C for 300 h. Additionally, carbon diffusion into the base material induces the
285 formation of TiC. Al-depletion has already been discussed as problematic for Cr₂AlC-bulk
286 materials. In their case the Al-consumption solely derives from Al-consumption due to oxide
287 formation. This phenomenon becomes even more severe for Cr₂AlC-coatings where Al-depletion
288 occurs in both directions. Comparable results were shown e.g. in [35] for the Cr₂AlC-coating on
289 pure Zr. Thermal exposure at 800°C led to Al-inward diffusion, pore formation, and finally the
290 thermal decomposition of the coating. In general, a high Al-activity a_{Al} (M-X covalent bonds
291 possess a higher binding energy than the respective M-A metallic bonds [8]) is an inherent feature
292 of the Al-containing MAX-phases and causes the required selective oxidation of Al. On the Zr
293 substrate, Al-inward diffusion accordingly occurred because of the high Al-concentration
294 gradient and insufficient thermodynamic stability of the Cr₂AlC/Zr-interface. In contrast, a
295 Cr₂AlC/AlN-interface could show the required long-term stability which makes AlN a potential
296 candidate for an efficient interdiffusion barrier (double-layer system). In our work, carbides form
297 during the thermal exposure and might have similar barrier properties, if applied as a first layer
298 before the MAX-phase coating.



299
 300 **Figure 10:** Proposed oxidation mechanism of the Cr_2AlC -based MAX-phase coating on the Ti4822 alloy as
 301 a function time.

302 **4.3. Mechanical properties**

303 Indentation hardness and modulus values of the Cr_2AlC -based coating match quite well to the
 304 values found in [48] and are both much higher compared to the TiAl base material. Comparably
 305 high values for the MAX-coating were also published in [49] and are characteristic for MS-
 306 coatings. Interestingly, hardness values of the coating are even higher compared to those
 307 published e.g. in [50] for Cr_2AlC -bulk materials which is given as 5.2 GPa. This distinctive
 308 difference could be explained by the so-called Hall-Patch effect since the number of grain
 309 boundaries is much higher in the (often nanocrystalline) coatings compared to bulk materials

310 leading to a certain strengthening effect [51]. Additionally, the precipitation of Cr-carbides and
311 Cr₂Al-phase, internal alumina or the existence of off-stoichiometric phases additionally can
312 contribute to this increase in hardness [52].

313 The results of the four-point-bending tests are very promising (Figure 9) , because they show, that
314 the initial fracture strain of the samples after annealing at 700°C is significantly higher compared
315 to e.g. pack aluminized samples as previously shown in an earlier study [5]. The columnar
316 morphology of the sputter coating clearly influences the fracture mode since cracks are initiated
317 primarily between the columns. Regarding this aspect, modification of the magnetron sputter
318 process (e.g. deposition at high temperatures) should have a clear influence on the microstructure
319 of the coating and could therefore change the fracture behavior. This should be investigated in the
320 future along with the potential use of a diffusion barrier underneath the MAX-phase.
321 Additionally, nanoporosity and internal oxidation shown by EMPA needs to be reduced, a finding
322 in line with [53]. Oxidation for 700°C and 800°C leads to a decrease in the fracture strain already
323 after 100 h caused by the stabilization of brittle Cr-carbides and the intermetallic Cr₂Al phase.
324 They are located primarily in the outermost area of the coating as well as along the columns and
325 therefore in those spots (the outermost fiber) which are under the highest tensile load during the
326 bending tests. Therefore, not only the long-term stability of the coating is negatively affected by
327 the Al-inward diffusion but also clearly the mechanical properties. The influence becomes even
328 more distinctive the higher the temperature and therefore the diffusion rates of Al are. In
329 comparison to the uncoated TiAl alloy much better mechanical properties are expected to exist
330 for the MAX-phase coated alloy for even longer exposure times.

331 Maintaining the microstructural stability of the coating by applying an interdiffusion barrier and
332 hindering Al from diffusing into the base material seems to be a promising approach in order to
333 retain the mechanical performance and should therefore be investigated in future studies.

334

335

336 **5. Conclusion**

337 The synthesis, oxidation resistance and mechanical properties of a Cr₂AlC-based MAX-Phase
338 coating on Ti4822 were investigated. The major findings can be summarized as follows:

- 339 • Cr₂AlC-based coatings with a columnar morphology were successfully synthesized by a
340 combination of DC magnetron sputtering and ex-situ heat treatment at 700°C for 1 h in Ar.
341 In addition to Cr₂AlC, Cr₇C₃ and Cr₂Al form primarily along the columns as well as the
342 coating/substrate-interface.
- 343 • After high temperature oxidation, an intermixed TiO₂/Al₂O₃-scale exists on top of the
344 uncoated Ti4822 alloy while for the Cr₂AlC-phase coated samples an extremely thin, well-
345 protective Al₂O₃+Cr₂O₃-scale forms leading to much lower overall mass gains especially at
346 800°C.
- 347 • Al-inward diffusion from the Cr₂AlC-coating into the substrate occurred and led to the
348 stabilization of Cr₇C₃, Cr₂₃C₆ as well as Cr₂Al.
- 349 • Mechanical properties of the coated samples are very promising in the initial condition
350 but are negatively affected by the successive thermal decomposition of the coating.

351

352 **Acknowledgements**

353 The authors thank the Federation of Industrial Cooperative Research Associations (AiF) for
354 funding this project (IGF grant 22355 N) as well as the analytical and metallographic departments
355 from the DECHEMA-Forschungsinstitut. Last, but not least our very special thanks go to Ellen
356 Berghof-Hasselbacher. Not only for her great contribution within this work, but more importantly
357 for her incessant help and passionate contribution to a vast number of publications throughout
358 the last decades. This work is dedicated to her.

359

360

361 **References**

362

- 363 [1] S. Mayer, P. Erdely, F. D. Fischer, D. Holec, M. Kasthuber, T. Klein, H. Clemens,
364 "Intermetallic β -Solidifying γ -TiAl Based Alloys – From Fundamental Research to
365 Application," *Adv. Eng. Mater.*, vol. 19, no. 4, pp. 1–27, 2017.
- 366 [2] B. P. Bewlay, S. Nag, A. Suzuki, M. J. Weimer, "TiAl alloys in commercial aircraft engines,"
367 *Mater. High Temp.*, vol. 33, no. 4–5, pp. 549–559, 2016.
- 368 [3] E. H. Copland, B. Gleeson, D. J. Young, "Formation of Z-Ti₅₀Al₃₀O₂₀ in the sub-oxide zones
369 of γ -TiAl-based alloys during oxidation at 1000 °C," *Acta Mater.*, vol. 47, no. 10, pp. 2937–
370 2949, 1999.
- 371 [4] E. Dettenwanger, E. Schumann, J. Rakowski, G. H. Meier, M. Rühle, "Development and
372 Microstructure of the Al-Depleted Layer of Oxidized TiAl," *Oxid. Intermet.*, vol. 27, 1996.
- 373 [5] L. Mengis, C. Oskay, A. Donchev, M. C. Galetz, "Critical assessment of the cyclic oxidation
374 resistance of the aluminized Ti-48Al-2Cr-2Nb TiAl alloy at 700 °C and its impact on
375 mechanical properties," *Surf. Coat. Technol.*, vol. 406, 2021.
- 376 [6] R. Pflumm, S. Friedle, M. Schütze, "Oxidation protection of γ -TiAl-based alloys - A review,"
377 *Intermetallics*, vol. 56, pp. 1–14, 2015.
- 378 [7] J. L. Smialek, "Oxidation behaviour of TiAl₃ coatings and alloys," *Corros. Sci.*, vol. 35, no. 5–
379 8, pp. 1199–1208, 1993.
- 380 [8] M. Radovic, M. W. Barsoum, "MAX phases: Bridging the gap between metals and
381 ceramics," *Amer. Ceram. Soc. Bull.*, vol. 92, no. 3, pp. 20–27, 2013.
- 382 [9] M. W. Barsoum, "The MAX Phases: Unique New Carbide and Nitride Materials," *Amer. Sci.*,
383 vol. 89, no. 4, pp. 334–343, 2013.
- 384 [10] J. Gonzalez-Julian, "Processing of MAX phases: From synthesis to applications," *J. Amer.*
385 *Ceram. Soc.*, pp. 1–32, 2020.

- 386 [11] D. B. Lee, T. D. Nguyen, S. W. Park, "Long-Time Oxidation of Cr₂AlC between 700 and
387 1,000 °C in Air," *Oxid. Met.*, vol. 77, no. 5–6, pp. 275–287, 2012.
- 388 [12] J. L. Smialek, "Oxidation of Al₂O₃ Scale-Forming MAX Phases in Turbine Environments,"
389 *Metall. Mater. Trans. A Phys. Metall. Mater. Sci.*, vol. 49, no. 3, pp. 782–792, 2018.
- 390 [13] T. Go, R. Vaßen, O. Guillon, J. Gonzalez-Julian, "Processing and oxidation response of
391 Cr₂AlC MAX-phase composites containing ceramic fibers," *Open Ceramics*, vol. 6, 2021.
- 392 [14] A. Shamsipoor, M. Farvizi, M. Razavi, A. Keyvani, B. Mousavi, "Comparison of the High-
393 Temperature Oxidation Behavior of Cr₂AlC MAX Phase and CoNiCrAlY Compounds,"
394 *Oxid. Met* **95**, pp. 1-21, 2021.
- 395 [15] A. Shamsipoor, M. Farvizi, M. Razavi, A. Kwyvani, B. Mousavi, W. Pan, "High-temperature
396 oxidation behaviour in YSZ coated Cr₂AlC and CoNiCrAlY substrates," *Surf. Coat. Tech.*,
397 vol. 401, 2020.
- 398 [16] P. Eklund, M. Beckers, U. Jansson, H. Högberg, L. Hultman, "The M_n+₁AX_n phases:
399 Materials science and thin-film processing," *Thin Solid Films*, vol. 518, no. 8, pp. 1851–1878,
400 2010.
- 401 [17] C. Tang, M. Steinbrueck, M. Stueber, M. Grosse, X. Yu, S. Ulrich, H. J. Seifert, "Deposition ,
402 characterization and high-temperature steam oxidation behavior of single-phase Ti₂AlC-
403 coated Zircaloy-4," *Corros. Sci.*, vol. 135, no. May 2017.
- 404 [18] Q. M. Wang, A. F. Renteria, O. Schroeter, R. Mykhaylonka, C. Leyens, W. Garkas, M. to
405 Baben, "Fabrication and oxidation behavior of Cr₂AlC coating on Ti6242 alloy," *Surf.*
406 *Coatings Technol.*, vol. 204, no. 15, pp. 2343–2352, 2010.
- 407 [19] A. Abdulkadhim, M. to Baben, T. Takahasi, V. Schnabel, H. Hans, C. Polzer, P. Polcik, J. J.
408 Schneider, "Crystallization kinetics of amorphous Cr₂AlC thin films," *Surf. Coat. Technol.*,
409 vol. 206, no. 4, pp. 599–603, 2011.

410

- 411 [20] B. Stelzer, X. Chen, P. Bliem, M. Hansm B. Böler, R. Sahu, C. Scheu, P. Primetzhifer, J. M.
412 Schneider, "Remote Tracking of Phase Changes in Cr₂AlC Thin Films by In-situ Resistivity
413 Measurements," *Sci. Rep.*, vol. 9, no. 1, 2019.
- 414 [21] Z. Feng, P. Ke, A. Wang, "Preparation of Ti₂AlC MAX Phase Coating by DC Magnetron
415 Sputtering Deposition and Vacuum Heat Treatment," *J. Mater. Sci. Technol.*, 2015.
- 416 [22] Q. Wang, W. Garkas, A. F. Renteria, C. Leyens, C. Sun, K. Kim, "Oxidation behaviour of a
417 Ti₂AlN MAX-phase coating," *IOP Conf. Ser. Mater. Sci. Eng.*, vol. 18, pp. 1–6, 2011.
- 418 [23] N. Laska, P. Bauer, O. Helle, F. Kreps, "Sputtering and Characterization of MAX-Phase
419 Forming Cr–Al–C and Ti–Al–C Coatings and Their Application on γ -Based Titanium
420 Aluminides," *Adv. Eng. Mater.*, vol. 2100722, pp. 1–10, 2021.
- 421 [24] C. Oskay, M. C. Galetz, H. Murakami, "Mechanical behaviour of conventional, Pt- and Pt/Ir-
422 modified NiAl diffusion coatings after thermocyclic exposure at 1100°C," *Mater. High
423 Temp.*, vol. 36, no. 5, pp. 404–416, 2019.
- 424 [25] J. A. Thornton, "High Rate Thick Film Growth," *Annu. Rev. Mater. Sci.*, vol. 7, pp. 239–260,
425 1977.
- 426 [26] L. Mengis, A. S. Ulrich, P. Watermeyer, C. H. Liebscher, M. C. Galetz, "Oxidation Behaviour
427 and Related Microstructural Changes of two β_0 -phase containing TiAl Alloys between 600
428 °C and 900 °C," *Corros. Sci.*, vol. 178, 2020.
- 429 [27] J. Gonzalez-Julian, G. Mauer, D. Sebold, D. E. Mack, R. Vaßen, "Cr₂AlC MAX phase as bond
430 coat for thermal barrier coatings: Processing, testing under thermal gradient loading, and
431 future challenges," *J. Amer. Ceram. Soc.*, vol. 103, no. 4, 2020.
- 432 [28] H. Clemens, S. Mayer, "Intermetallic titanium aluminides in aerospace applications -
433 processing, microstructure and properties," *Mater. High Temp.*, vol. 22, no. 4-5, pp. 560-570,
434 2016.

435

- 436 [29] M. Ougier, A. Michau, F. Schuster, H. Maskrot, M. L. Schlegel, "Effects of HiPIMS
437 discharges and annealing on Cr-Al-C thin films," *Surf. Coat. Technol.*, vol. 399, 2020.
- 438 [30] A. Abdulkadhim, T. Takahashi, D. Music, F. Munnik, J. M. Schneider, "MAX phase
439 formation by intercalation upon annealing of TiC_x/Al(0.4≤x≤1) bilayer thin films," *Acta*
440 *Mater.*, vol. 59, no. 15, pp. 6168–6175, 2011.
- 441 [31] L. Gröner, L. Mengis, M. C. Galetz, L. Kirste, P. Daum, M. Wirth, F. Meyer, A. Fromm, B.
442 Blug, F. Burmeister, "Investigations of the Deuterium Permeability of As-Deposited and
443 Oxidized Ti₂AlN Coatings," *Materials* 2020, 13(9), 2085.
- 444 [32] R. Boucher, O. Berger, C. Leyens, "Magnetic properties of bulk and thin film Cr-Al-C
445 compounds", *Surf. Eng.* 32:3, 172-177,2016.
- 446 [33] D. E. Hajas, M. To Baben, B. Hallstedt, R. Iskandar, J. Mayer, J. M. Schneider, "Oxidation of
447 Cr₂AlC coatings in the temperature range of 1230 to 1410°C," *Surf. Coat. Technol.*, vol. 206,
448 no. 4, pp. 591–598, 2011.
- 449 [34] M. Fröhlich, "Investigations on the Oxidation Behavior of Max-Phase Based Ti₂AlC
450 Coatings on γ-TiAl," in: *Ceram. Eng. Sci. Proceed.*, pp. 161–169, 2010.
- 451 [35] S. Mráz, M. Tyra, M. to Baben, M. Hans, C. Chen, F. Herrig, K. Lambrinou, J. M. Schneider,
452 "Thermal stability enhancement of Cr₂AlC coatings on Zr by utilizing a double layer
453 diffusion barrier," *J. Eur. Ceram. Soc.*, vol. 40, no. 4, pp. 1119–1124, 2020.
- 454 [36] J. C. Schuster, H. Nowotny, C. Vaccaro, "The ternary systems: Cr–Al–C, V–Al–C, and Ti–
455 Al–C and the behavior of H-phases (M₂AlC)," *J. Solid State Chem.*, vol. 32, no. 2, pp. 213–219,
456 1980.
- 457 [37] R. Mertens, Z. Sun, D. Music, J. M. Schneider, "Effect of the composition on the structure of
458 Cr-Al-C investigated by combinatorial thin film synthesis and ab initio calculations," *Adv.*
459 *Eng. Mater.*, vol. 6, no. 11, pp. 903–907, 2004.

460

- 461 [38] F. Dettenwanger, E. Schumann, M. Rühle, J. Rakowski, G. H. Meier, "Microstructural study
462 of oxidized γ -TiAl," *Oxid. Met.*, vol. 50, no. 3–4, pp. 269–307, 1998.
- 463 [39] M. Schütze, "The Role of Surface Protection for High-Temperature Performance of TiAl
464 Alloys," *JOM*, vol. 69, no. 12, pp. 2602–2609, 2017.
- 465 [40] M. C. Galetz, A. S. Ulrich, C. Oskay, N. Laska, U. Schulz, M. Schütze, "Oxidation-induced
466 microstructural changes of the TiAl TNM-B1 alloy after exposure at 900 °C in air,"
467 *Intermetallics*, vol. 123, 2020.
- 468 [41] A. Rahmel, P. J. Spencer, "Thermodynamic aspects of TiAl and TiSi₂ oxidation: The Al-Ti-
469 O and Si-Ti-O Phase diagrams," *Oxid. Met.* **35**, no. 1–2, pp. 53–68, 1991.
- 470 [42] P. Kofstad, "Note on the defect structure of rutile (TiO₂)," *J. Less-Common Met.*, vol. 13, no.
471 6, pp. 635–638, 1967.
- 472 [43] P. Sallot, J. P. Monchoux, S. Joulié, A. Couret, M. Thomas, "Impact of β -phase in TiAl alloys
473 on mechanical properties after high temperature air exposure," *Intermetallics*, vol. 119, 2020.
- 474 [44] I. E. Locci, M. P. Brady, R. A. MacKay, J. W. Smith, "Very long term oxidation of Ti-48Al-
475 2Cr-2Nb at 704°C in air," *Scr. Mater.*, vol. 37, no. 6, pp. 761–766, 1997.
- 476 [45] D. B. Lee, "Critical Review of the Oxidation of Cr₂AlC," *Adv. Sci. Technol.*, vol. 89, pp. 115–
477 122, 2014.
- 478 [46] H. J. Yang, X. H. Shao, Y. T. Pei, Z. F. Zhang, J. T. M. De Hosson, "Enhanced efficiency of
479 self-healing of Cr₂AlC," *Mater. Lett.*, vol. 227, pp. 51–54, 2018.
- 480 [47] H. Asteman, M. Spiegel, "A comparison of the oxidation behaviours of Al₂O₃ formers and
481 Cr₂O₃ formers at 700 °C - Oxide solid solutions acting as a template for nucleation," *Corros.*
482 *Sci.*, vol. 50, no. 6, pp. 1734–1743, 2008.
- 483 [48] J. M. Schneider, D. P. Sigumonrong, D. Music, C. Walter, J. Emmerlich, R. Iskandar, J.
484 Mayer, "Elastic properties of Cr₂AlC thin films probed by nanoindentation and ab initio
485 molecular dynamics," *Scr. Mater.*, vol. 57, pp. 1137–1140, 2007.

- 486 [49] M. W. Qureshi, X. Ma, G. Tang, B. Miao, and J. Niu, "Fabrication and mechanical properties
487 of Cr₂AlC max phase coatings on TiBw/Ti6Al4V composite prepared by HiPIMS," *Materials*,
488 vol. 14, no. 4, pp. 1–22, 2021.
- 489 [50] W. B. Tian, P. L. Wang, G. J. Zhang, Y. M. Kan, Y. X. Li, "Mechanical properties of Cr₂AlC
490 ceramics," *J. Am. Ceram. Soc.*, vol. 90, no. 5, pp. 1663–1666, 2007.
- 491 [51] N. Hansen, "Hall-petch relation and boundary strengthening," *Scr. Mater.*, vol. 51, no. 8, pp.
492 801–806, 2004.
- 493 [52] Y. L. Su, Y. F. Lin, "Microstructure, phase transformation and hardness of nanometric Cr-
494 Al multilayer coatings," *Adv. Mech. Eng.*, vol. 7, no. 6, pp. 1–7, 2015.
- 495 [53] X. Chen, B. Stelzer, M. Hans, R. Iskandar, J. Mayer, J. M. Schneider, "Enhancing the high
496 temperature oxidation behavior of Cr₂AlC coatings by reducing grain boundary
497 nanoporosity," *Mater. Res. Lett.*, vol. 9, no. 3, pp. 127–133, 2021.

498